The interphase elasto-plastic damaging model

Giuseppe Giambanco[1,*], Giuseppe Fileccia Scimemi[1], Antonino Spada[1]

[1] Department of Civil, Environmental, Aerospace and Materials' Engineering, University of Palermo, 90128, Italy
* Corresponding author: giuseppe.giambanco@unipa.it

Abstract Heterogeneous materials present a mechanical response strongly dependent on the static and kinematic phenomena occurring in the constituents and at their joints. In order to analyze this kind of materials it is a common practice to distinguish a macroscopic length scale of interest from a mesoscopic one, where the mesoscopic length scale is of the order of the typical dimensions of the constituents. At the mesoscopic level the interaction between the units is simulated by mean of apposite mechanical devices. Among these devices is popular the zero thickness interface model where contact tractions and displacement discontinuities are the primary static and kinematic variables respectively. However, in heterogeneous materials the response also depends on joint internal stresses as much as on contact stresses. The introduction of internal stresses brings to the interphase model or an enhancement of the classical zero-thickness interface. With the term 'interphase' we shall mean a layer separated by two physical interfaces from the bulk material or a multilayer structure with varying properties and several interfaces. Different failure conditions can be introduced for the physical interfaces and for the joint material. The interphase model has been implemented in an open-source research-oriented finite element analysis program for 2D applications. Numerical simulations are provided to show the main features of the model.

Keywords Interphase element, Damage, Elastoplasticity, Finite element

1. Introduction

The mechanical response of all those structures that are constituted by heterogeneous materials is dependent by different static and kinematic phenomena occurring in each constituent and at their joints. Material degradation due to nucleation, growth and coalescence of microvoids and microcracks is usually accompanied by plastic deformations as decohesion and sliding that cause strain softening and induced anisotropy.

The mesoscopic approach is by now the most diffused technique to understand this kind of materials, because it overcomes the problems associated with the strong simplifications that have to be introduced when the macroscopic approach is applied. In particular, with the mesoscopic approach all the material constituents are modelled individually and their interactions are regulated by using appropriate devices able to reproduce the inelastic phenomena that usually occur at the physical interfaces. In literature, these mechanical devices are generally called contact elements, normally distinguished between link elements, thin layer elements and zero-thickness interface elements (ZTI). In the last decades interface elements have been applied in several engineering applications due to their simple formulation and to their easiness to be implemented in finite element codes [1-10].

The interface constitutive laws are expressed in terms of contact tractions and displacement discontinuities which are considered as generalized joints strains. In order to model the nonlinear behaviour caused by plastic deformations and damage evolution the constitutive laws of the interface elements are formulated making use of concepts borrowed by theory of Plasticity and Continuum Damage Mechanics.

In many cases the structural response depends also on internal stresses and strains within the joint. It is sufficient to think to the fracture that appears in the middle of masonry blocks caused by the horizontal tangential contact stresses between the mortar and the block when a masonry assembly is subjected to a pure compressive load. These tangential stresses cannot be captured by the classical ZTI model. Therefore, the usual assumption used in zero-thickness interface elements, where the response is governed by contact stress components, may require a correction by introducing the

effect of the internal stresses into the analysis. This enhancement of the ZTI is known as interphase model, for the first time proposed by Giambanco and Mròz [11].
The interphase element has been formulated by authors as a new contact element and introduced in a scientific oriented finite element code. Patch tests have been carried out in elasticity to investigate the numerical performance and convergence of the element. All the results are shown in the paper written by Giambanco el al. [12]. In particular, in that paper is shown how strategies such as the Reduced Selective Integration or the Enhanced Assumed Strain methods are necessary to avoid shear locking effects of the element.
In this work the interphase element is implemented for nonlinear applications by introducing separate limit conditions for the joint bulk material and for the physical interfaces. In particular the damage mechanics theory is used to simulate the formation and propagation of fractures in the bulk material. The elastoplastic limit condition of Mohr-Coulomb type with a tensile cut-off is adopted to describe the decohesion process of the interfaces. The contact strains are subdivided in an elastic and a plastic part. The overall model is thermodynamically consistent and the flow rules are derived by applying the Lagrangian method. With the aim to show the effectiveness of the model the interphase constitutive laws have been implemented in an open-source research-oriented finite element analysis program for 2D applications and by using the Selective Reduced Integration.
The paper is organized as follows. In Section 2 the general assumptions of the model are reported and the expression of the Helmholtz free energy is furnished. In Section 3 the state equations and the flow rules are determined on the base of the thermodynamically consistent theory. Section 4 is finally dedicated to numerical applications in order to show the effectiveness of the proposed model.

2. General assumptions and Thermodynamics.

Let us consider, in the Euclidean space $\Re^3$ referred to the orthonormal frame $(O,\mathbf{i_1},\mathbf{i_2},\mathbf{i_3})$, a structure formed by two adherents Ω^+, Ω^- connected by a third material Ω in contact with the two bodies by means of the two physical interfaces Σ^+ and Σ^- respectively, as in Fig. 1.

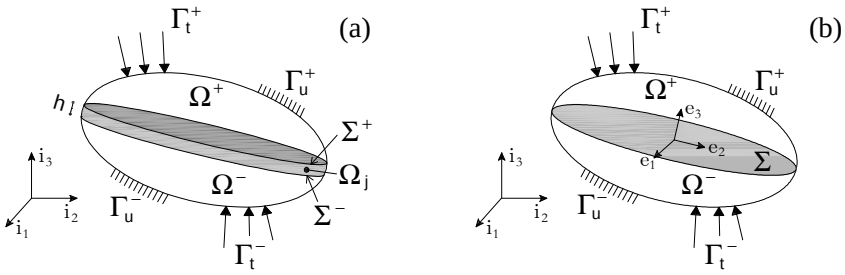

Figure 1. (a) Mechanical scheme of a third body interposed between two adherents;
(b) Interphase mechanical scheme.

It is assumed that the thickness h of the joint is small if compared with the characteristic dimensions of the bonded assembly.
The boundary of the two adherents is divided in the two parts $\Gamma_u^{\pm}$ and $\Gamma_t^{\pm}$, where kinematic and loading conditions are specified respectively.
The joint interacts with the two adherents through the following traction components:

$$\mathbf{t}^{\pm} = t_1^{\pm}\mathbf{e}_1 + t_2^{\pm}\mathbf{e}_2 + t_3^{\pm}\mathbf{e}_3 \tag{1}$$

which can be considered as the external surface loads for the joint.

In Eq. (1) $\mathbf{e}_1$, $\mathbf{e}_2$ and $\mathbf{e}_3$ are the unit vectors of the local reference system, with $\mathbf{e}_3$ oriented along the normal to the middle surface Σ and directed towards the adherent Ω^+.
The joint can be regarded as an interphase model. It is assumed that the fibers inside the interphase and directed along $\mathbf{e}_3$ are maintained rectilinear during the deformation process. In view of this hypothesis the interphase displacement field $\mathbf{u}$ can be easily obtained from the displacement $\mathbf{u}^+$ and $\mathbf{u}^-$ of the interfaces Σ^+ and Σ^-, thus

$$\mathbf{u}(x_1, x_2, x_3) = \left(\frac{1}{2} + \frac{x_3}{h}\right)\mathbf{u}^+\left(x_1, x_2\right) + \left(\frac{1}{2} - \frac{x_3}{h}\right)\mathbf{u}^-\left(x_1, x_2\right) \tag{2}$$

with x_1, x_2 and x_3 the Cartesian coordinates in the orthonormal frame $\left(O, \mathbf{e}_1, \mathbf{e}_2, \mathbf{e}_3\right)$.
Since the thickness of the joint is generally small if compared to the characteristic dimensions of the adherents, we can assume the strain state $\boldsymbol{\varepsilon}$ uniform along the $\mathbf{e}_3$ direction and given by:

$$\boldsymbol{\varepsilon}(x_1, x_2) = \frac{1}{h}\int_{-h/2}^{h/2} \nabla^s \mathbf{u}\left(x_1, x_2, x_3\right) dx_3 \tag{3}$$

Substituting the Eq. (2) we have:

$$\boldsymbol{\varepsilon}(x_1, x_2) = \frac{1}{2h}\left(\left[\mathbf{u}\right] \otimes \mathbf{n} + \mathbf{n} \otimes \left[\mathbf{u}\right]\right) + \frac{1}{2}\nabla^s\left(\mathbf{u}^+ + \mathbf{u}^-\right) \tag{4}$$

where $\left[\mathbf{u}\right] = \mathbf{u}^+ - \mathbf{u}^-$, $\mathbf{n}$ is the unit normal vector to the interphase plane and ∇^s is the symmetric gradient operator defined as $\nabla^s = \frac{1}{2}\left(\nabla + \nabla^T\right)$.
Let us note that in the interphase model the joint curvatures generated by displacement field (2) and the related flexural effect are neglected.
Equilibrium equations are derived by applying the principle of virtual displacements (PVD) that asserts that the external work produced by the contact tractions equals the internal work developed in the joint. According to the hypothesis of a constant strain state, by applying the divergence theorem and assuming that $\Sigma = \Sigma^+ = \Sigma^-$, the PVD leads to the following local equilibrium relations of the interphase model:

$$\mathbf{t}^+ - \boldsymbol{\sigma}\cdot\mathbf{n} + \frac{h}{2} div\boldsymbol{\sigma} = \mathbf{0}; \quad \mathbf{t}^- + \boldsymbol{\sigma}\cdot\mathbf{n} + \frac{h}{2} div\boldsymbol{\sigma} = \mathbf{0} \quad on\ \Sigma, \tag{5}$$

$$\mathbf{m}\cdot\boldsymbol{\sigma} = \mathbf{0} \quad on\ \Gamma. \tag{6}$$

The basic kinematical hypotheses are the additive decomposition of total strain in the internal (*i*) and contact (*c*) parts and, for the contact strain only, a further decomposition in elastic (*e*) and inelastic (*p*) parts:

$$\boldsymbol{\varepsilon} = \boldsymbol{\varepsilon}^i + \boldsymbol{\varepsilon}^c \tag{7}$$

$$\boldsymbol{\varepsilon}^c = \boldsymbol{\varepsilon}^{ce} + \boldsymbol{\varepsilon}^{cp} \tag{8}$$

with

$$\boldsymbol{\varepsilon}^i = \mathbf{A}\boldsymbol{\varepsilon}\mathbf{A} \tag{9}$$

being $\mathbf{A} = \mathbf{I} - \mathbf{n}\otimes\mathbf{n}$ the unit second order tensor.
In order to comply with thermodynamic requirements, the interphase Helmholtz free energy is introduced in the following form:

$$\Psi\left(\boldsymbol{\varepsilon}^i, \boldsymbol{\varepsilon}^c, \boldsymbol{\varepsilon}^{cp}, \boldsymbol{\omega}, \xi_d, \xi_p\right) = \Psi^i\left(\boldsymbol{\varepsilon}^i, \boldsymbol{\omega}, \xi_d\right) + \Psi^c\left(\boldsymbol{\varepsilon}^c, \boldsymbol{\varepsilon}^{cp}, \xi_p\right) + \Psi^{i,c}\left(\boldsymbol{\varepsilon}^i, \boldsymbol{\varepsilon}^c, \boldsymbol{\varepsilon}^{cp}, \boldsymbol{\omega}\right); \tag{10}$$

where Ψ^i and Ψ^c represent the free energies related to the internal and contact parts of the strain state respectively and Ψ^{ic} is the mixed term of the free energy which takes into account the co-presence of the contact and internal strains. ξ_d and ξ_p are the damage and plastic internal variables, respectively.

The principle considered for developing the constitutive laws is that damage occurs in the bulk material, therefore the damage tensor $\boldsymbol{\omega}$ appears in the two terms of the total free energy that are functions of the internal strains also. In this way the constitutive model takes into account the onset of microvoids and fractures along the thickness of the joint. On the other hand, debonding of the joint from the adherents, sliding and fractures developing on surfaces parallel to the middle plane of the interphase are modelled using elastoplasticity and the inelastic contact strains $\boldsymbol{\varepsilon}^{cp}$ are the related internal variables.

In this work a single scalar damage variable ω governs the loss of stiffness of the bulk material. It ranges from 0 to 1, with the inferior and superior limits having the meaning of a pristine and a fully damaged bulk material, respectively.

The explicit expression of the components of the free energy is given below:

$$\Psi^i = \frac{1}{2}(1-\omega)\left[\lambda \operatorname{tr}^2\left(\boldsymbol{\varepsilon}^i\right) + 2\mu\,\boldsymbol{\varepsilon}^i : \boldsymbol{\varepsilon}^i\right] - h_d\left[\xi_d + \ln\left(1-\xi_d\right)\right] \tag{11}$$

$$\Psi^c = \frac{1}{2}\left[\lambda \operatorname{tr}^2\left(\boldsymbol{\varepsilon}^c - \boldsymbol{\varepsilon}^{cp}\right) + 2\mu\left(\boldsymbol{\varepsilon}^c - \boldsymbol{\varepsilon}^{cp}\right) : \left(\boldsymbol{\varepsilon}^c - \boldsymbol{\varepsilon}^{cp}\right)\right] + \frac{1}{2}h_p\xi_p^2 \tag{12}$$

$$\Psi^{i,c} = (1-\omega)\,\lambda \operatorname{tr}\left(\boldsymbol{\varepsilon}^{\mathrm{i}}\right)\operatorname{tr}\left(\boldsymbol{\varepsilon}^{\mathrm{c}} - \boldsymbol{\varepsilon}^{\mathrm{cp}}\right) \tag{13}$$

where λ and μ are the Lamè's constants, h_d is a material parameter which governs the softening response associated to the damage onset and growth, and h_p is a material parameter specifying isotropic hardening/softening interface response.

3. State equations and flow rules.

In order to derive the interphase constitutive equations, the second principle of thermodynamics, taking into account also the balance equation (first principle) can be applied in the form of the Clausius-Duhem inequality. This inequality for isothermal purely mechanical evolutive process reads as

$$D = \boldsymbol{\sigma} : \dot{\boldsymbol{\varepsilon}} - \dot{\Psi} \geq 0 \tag{14}$$

where D is the interphase dissipation (for unit surface) or net entropy production.

From the assumed form of the Helmholtz free energy (Eq. 10) its general rate has the following expression:

$$\begin{aligned}\dot{\Psi} = &\left(\frac{\partial \Psi^i}{\partial \boldsymbol{\varepsilon}^i} + \frac{\partial \Psi^{i,c}}{\partial \boldsymbol{\varepsilon}^i}\right) : \dot{\boldsymbol{\varepsilon}}^i + \left(\frac{\partial \Psi^c}{\partial \boldsymbol{\varepsilon}^c} + \frac{\partial \Psi^{i,c}}{\partial \boldsymbol{\varepsilon}^c}\right) : \dot{\boldsymbol{\varepsilon}}^c + \left(\frac{\partial \Psi^c}{\partial \boldsymbol{\varepsilon}^{cp}} + \frac{\partial \Psi^{i,c}}{\partial \boldsymbol{\varepsilon}^{cp}}\right) : \dot{\boldsymbol{\varepsilon}}^{cp} + \\ &+ \left(\frac{\partial \Psi^i}{\partial \omega} + \frac{\partial \Psi^{i,c}}{\partial \omega}\right) : \dot{\omega} + \frac{\partial \Psi^i}{\partial \xi_d}\dot{\xi}_d + \frac{\partial \Psi^c}{\partial \xi_p}\dot{\xi}_p\end{aligned} \tag{15}$$

Particularizing Eq. (14) for a purely elastic incremental deformation process ($\dot{\boldsymbol{\varepsilon}}^{cp} = \mathbf{0}$, $\dot{\omega} = \dot{\xi}_d = \dot{\xi}_p = 0$), assuming the decomposition of the stress state similar to that used for the strain state

$$\boldsymbol{\sigma} = \boldsymbol{\sigma}^i + \boldsymbol{\sigma}^c, \qquad \text{being} \qquad \boldsymbol{\sigma}^i = \mathbf{A}\boldsymbol{\sigma}\mathbf{A} \tag{16}$$

and considering the adopted expressions of the free energy parts (Eq. 11-13), the elastic stress-strain equations can be derived, thus

$$\sigma^i = (1-\omega)\left\{\lambda\left[\operatorname{tr}\left(\boldsymbol{\varepsilon}^i\right) + \operatorname{tr}\left(\boldsymbol{\varepsilon}^c - \boldsymbol{\varepsilon}^{cp}\right)\right]\mathbf{A} + 2\mu\boldsymbol{\varepsilon}^i\right\} \tag{17}$$

$$\sigma^c = \lambda\left[(1\text{-}\omega)\operatorname{tr}\left(\boldsymbol{\varepsilon}^i\right) + \operatorname{tr}\left(\boldsymbol{\varepsilon}^c - \boldsymbol{\varepsilon}^{cp}\right)\right](\mathbf{I}-\mathbf{A}) + 2\mu\left(\boldsymbol{\varepsilon}^c - \boldsymbol{\varepsilon}^{cp}\right) \tag{18}$$

$$\chi_p = h_p\xi_p \tag{19}$$

$$\chi_d = h_d\frac{\xi_d}{1-\xi_d} \tag{20}$$

$$\zeta = \frac{1}{2}\left[\lambda\operatorname{tr}^2\left(\boldsymbol{\varepsilon}^i\right) + 2\mu\,\boldsymbol{\varepsilon}^i : \boldsymbol{\varepsilon}^i\right] + \lambda\operatorname{tr}\left(\boldsymbol{\varepsilon}^i\right)\operatorname{tr}\left(\boldsymbol{\varepsilon}^c - \boldsymbol{\varepsilon}^{cp}\right) \tag{21}$$

where χ_p and χ_d are the static variables conjugate of the internal variables ξ_p and ξ_d respectively, and ζ the thermodynamic force conjugate of the damage variable ω.

Making use of the elastic strain-stress equation and of the previous positions, the final expression of the instantaneous dissipation is obtained:

$$D = \boldsymbol{\sigma}^c : \dot{\boldsymbol{\varepsilon}}^{cp} - \chi_p\dot{\xi}_p - \chi_d\dot{\xi}_d + \zeta\dot{\omega} \geq 0\,. \tag{22}$$

In order to regulate the activation of each dissipative mechanism, two different yield functions are defined in the space of the proper static variables, namely:

$$\Phi_p\left(\boldsymbol{\sigma}^c, \chi_p\right) \leq 0, \qquad \Phi_d\left(\zeta, \chi_d\right) \leq 0 \tag{23}$$

where Φ_p is the classical plastic yield function specifying the elastic contact domain assumed convex and Φ_d is the damage activation function also assumed convex.

The activation of each dissipation mechanism can be effectively described by a variational formulation which is represented by the generalized principle of maximum intrinsic dissipation:

$$\max_{\boldsymbol{\sigma}^c, \chi_p, \chi_d, \zeta}\left(\boldsymbol{\sigma}^c : \dot{\boldsymbol{\varepsilon}}^{cp} - \chi_p\dot{\xi}_p - \chi_d\dot{\xi}_d + \zeta\dot{\omega}\right) \tag{24}$$

subject to the constraints (Eq. 23). The Kuhn-Tucker conditions of the maximum constrained problem provide the plastic and damage evolution laws of the interphase:

$$\dot{\boldsymbol{\varepsilon}}^{cp} = \dot{\lambda}_p\frac{\partial\Phi_p}{\partial\boldsymbol{\sigma}^c}; \quad \dot{\omega} = \dot{\lambda}_d\frac{\partial\Phi_d}{\partial\zeta} \tag{25}$$

$$-\dot{\xi}_p = \dot{\lambda}_p\frac{\partial\Phi_p}{\partial\chi_p}; \quad -\dot{\xi}_d = \dot{\lambda}_d\frac{\partial\Phi_d}{\partial\chi_d} \tag{26}$$

$$\Phi_p\left(\boldsymbol{\sigma}^c, \chi_p\right) \leq 0, \quad \dot{\lambda}_p \geq 0, \quad \dot{\lambda}_p\Phi_p\left(\boldsymbol{\sigma}^c, \chi_p\right) = 0 \tag{27}$$

$$\Phi_d\left(\zeta, \chi_d\right) \leq 0, \quad \dot{\lambda}_d \geq 0, \quad \dot{\lambda}_d\Phi_d\left(\zeta, \chi_d\right) = 0 \tag{28}$$

being $\dot{\lambda}_p$ and $\dot{\lambda}_d$ the plastic and damage multiplier, respectively.

In the present study the elasto-plastic convex domain is defined by the intersection of the classical Mohr-Coulomb bilinear function with a tension cut-off:

$$\Phi_{p1}\left(\boldsymbol{\sigma}^c, \chi_p\right) = \left|\boldsymbol{\tau}^c\right| + \sigma^c \tan\varphi - c_0\left(1-\chi_p\right) \tag{29}$$

$$\Phi_{p2}\left(\boldsymbol{\sigma}^c, \chi_p\right) = \sigma^c - \sigma_0\left(1-\chi_p\right) \tag{30}$$

where $\boldsymbol{\tau}^c$ and σ^c are the tangential stress vector and the normal stress component of the contact stresses, φ is the friction angle, c_0 and σ_0 the cohesion and tensile strength of the virgin interfaces.

The two yield functions are depicted in Fig. 2. The following four zones can be distinguished:

I elastic zone: $\Phi_{p1} < 0, \quad \Phi_{p2} < 0$

II plastic activation in shear: $\Phi_{p1} = 0, \quad \Phi_{p2} < 0$

III plastic activation in tension: $\Phi_{p1} < 0, \quad \Phi_{p2} = 0$

IV plastic activation in tension and shear (corner): $\Phi_{p1} = 0, \quad \Phi_{p2} = 0$.

The damage activation function is linear and the first activation occurs when the thermodynamic force reaches the relative threshold value ζ_0:

$$\Phi_d\left(\zeta, \chi_d\right) = \zeta - \zeta_0\left(1-\chi_d\right) \tag{31}$$

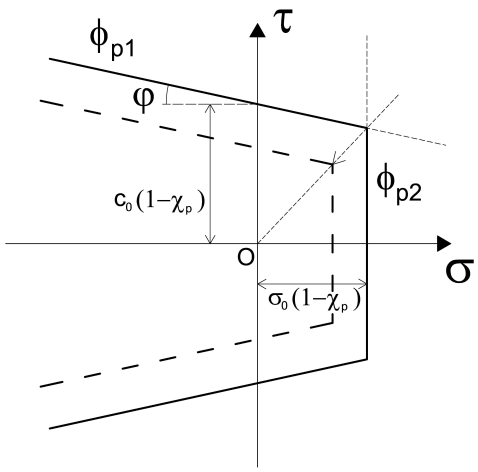

Figure 2. Plastic yield conditions represented in the stress space.

4. Numerical applications.

The interphase model presented in Sections 2 and 3 has been implemented in an open-source research-oriented finite element analysis program for 2D applications. With the aim to run a step-by-step integration, flow rules given in rate form were rewritten as discrete laws. The implicit backward-Euler difference method was applied to obtain results within the time step

$[t_n, \ t_{n+1}] \subset [0, \ T]$. In particular the nonlinear solution at time t_{n+1} has been calculated by means of an elastic prediction – plastic and/or damaging correction procedure. The interphase element has four nodes and zero-thickness. The integration of the stiffness matrix has been solved by applying the Reduced Selective Integration method, that is two Gauss are used for the integration in the direction normal to the interphase plane while one Gauss point is used in the tangential one.
The numerical applications presented in this work regard uniaxial compression and diagonal compression tests on masonry specimens. All numerical examples have been carried out under the hypothesis of plane stress state.

4.1. Uniaxial compression tests on masonry.

Uniaxial compression tests have been carried out to assess the performance of the interphase element. A brick-mortar-brick system uniformly compressed (Fig. 3) has been considered with the aim to show the formation of damage in the bulk material when the stiffness of the bricks is lower than that one of mortar. In this case, in fact, the bricks tend to expand more than the mortar in the horizontal direction because of the Poisson effect, but the higher stiffness of the mortar opposes to this displacement. The bricks are therefore subjected to compressive stresses while the mortar to tensile ones along the x-axis.

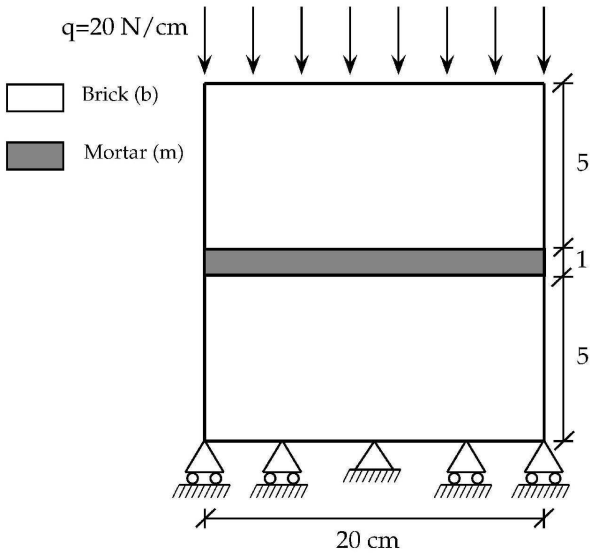

Figure 3. Uniaxial compression test on a masonry block.

The parameters used for tests are reported in Table 1, while the results are shown in Fig. 4. The numerical test has been performed under displacement control. In this paper the results obtained with a load multiplier equal to 3 and for a FE model with 80 interphase elements are reported in terms of stresses along the mortar layer.

Table 1. Parameters used for compression test.

E_{brick}	500 MPa	ν_{brick}	0.3
E_{mortar}	15000 MPa	ν_{mortar}	0.2
c_0	4.5 MPa	φ	30°
σ_0	1.0 MPa	h_p	1
ζ_0	0.001 MPa	h_d	0.0025 MPa

The diagrams depicted in Fig. 4 clearly show the points were the damage nucleation takes place. The first fracture forms in the middle of the layer and grows during the following steps. As a consequence, a redistribution of stresses takes place in the two parts on sides of the fracture. When the thermodynamic force in another Gauss point or group of Gauss points overcomes the threshold value a new fracture appears symmetrically with respect to the middle of the mortar joint. On the other hand, while σ_x stresses suddenly fall down and tend to zero, the σ_z values are little influenced by fracture. This is due to the fact that damage affects only internal and mixed terms of the free energy.

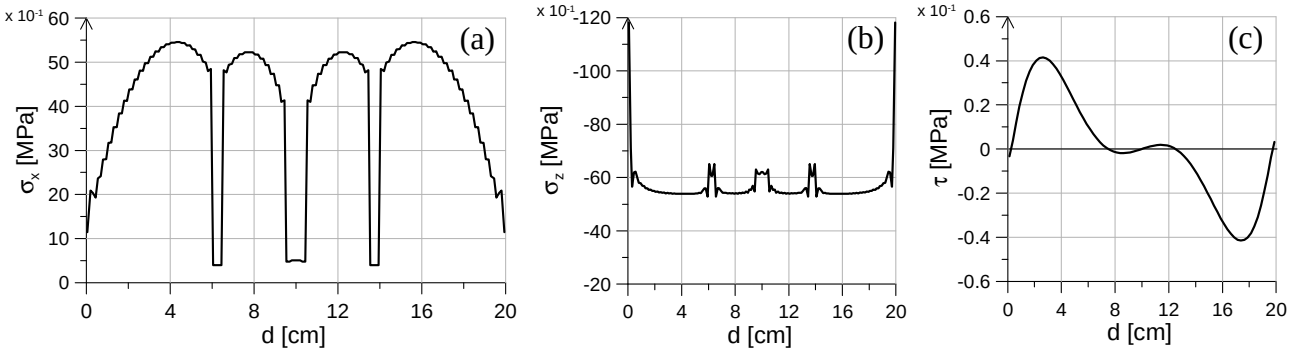

Figure 4. Uniaxial compression test on a masonry block: results at a load multiplier equal to 3. (a) normal stresses along x-axis; (b) vertical stresses; (c) tangential stresses.

4.2. Diagonal compression tests on masonry.

Diagonal compression numerical tests have been carried out on a masonry panel and compared with the experimental results obtained in laboratory. With reference to Fig. 5, the specimen is made up of four courses of sandstone blocks with calcium-cement mortar. It has a squared shape with a length of 67 cm for each side. A single block is 33 cm long and 16 cm high. The mortar layer has a thickness of 1 cm. A total number of 256 plane stress 2D solid elements and 72 interphase elements has been used to create the finite element model.

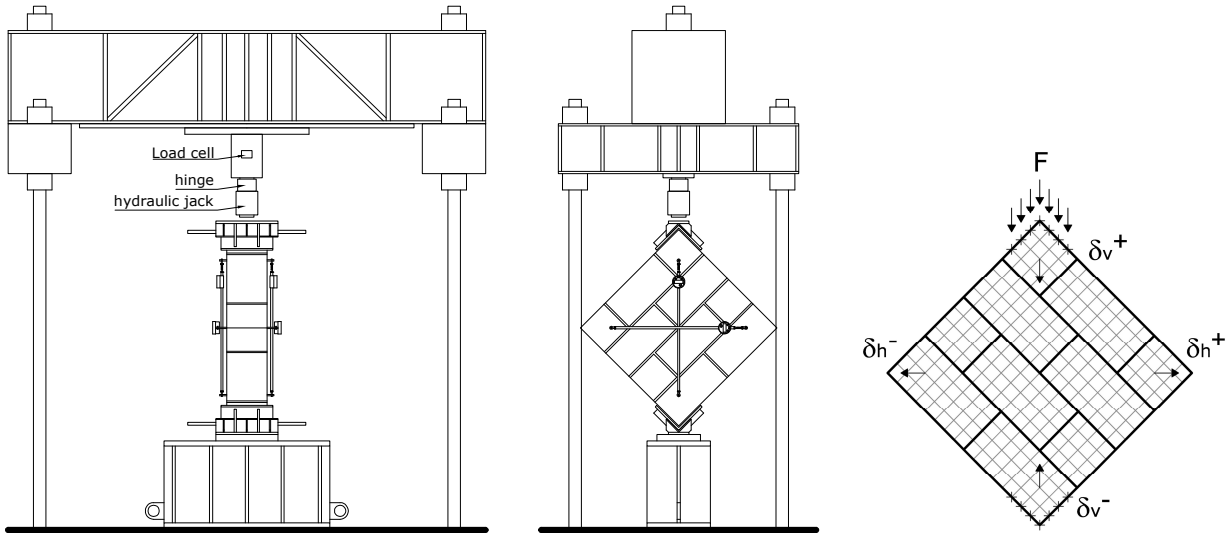

Figure 5. Diagonal compression test on a masonry panel. Experimental setup and finite element model.

The mechanical variables for blocks and mortar and the parameters used for the finite element model are reported in Table 2.

Table 2. Parameters used for diagonal compression test.

E_{brick}	11141.67 MPa	ν_{brick}	0.25
E_{mortar}	37000 MPa	ν_{mortar}	0.14
c_0	5.0 MPa	φ	35°
σ_0	1.0 MPa	h_p	0.04
ζ_0	$1 \cdot 10^{-5}$ MPa	h_d	0.001 MPa

The test has been run with 400 steps under displacement control. At each step the values of the total vertical load F and the displacement discontinuities $\delta h = \delta h^+ + \delta h^-$ and $\delta v = \delta v^+ + \delta v^-$, in horizontal and vertical direction respectively, have been evaluated and reported in the load-displacement curves of Fig. 6. A good agreement has been obtained with experimental results.

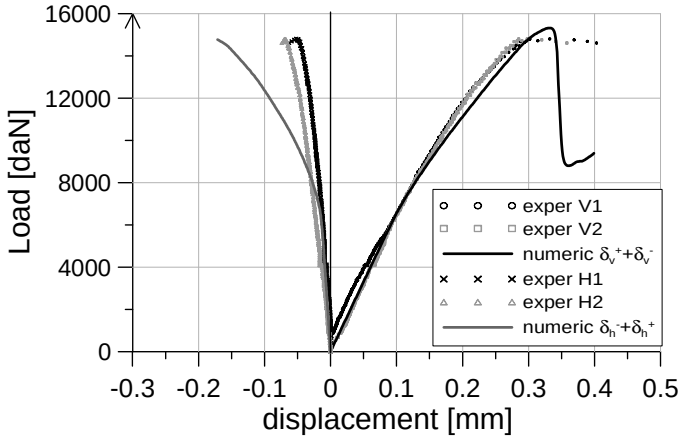

Figure 6. Load-displacement curves: comparison between numerical and experimental results.

Fig. 7 finally shows a comparison between the collapse experimental and numerical configurations. A very good agreement can be observed, even if the numerical model is not able to simulate the fracture inside the blocks because an elastic behavior was chosen for bricks.

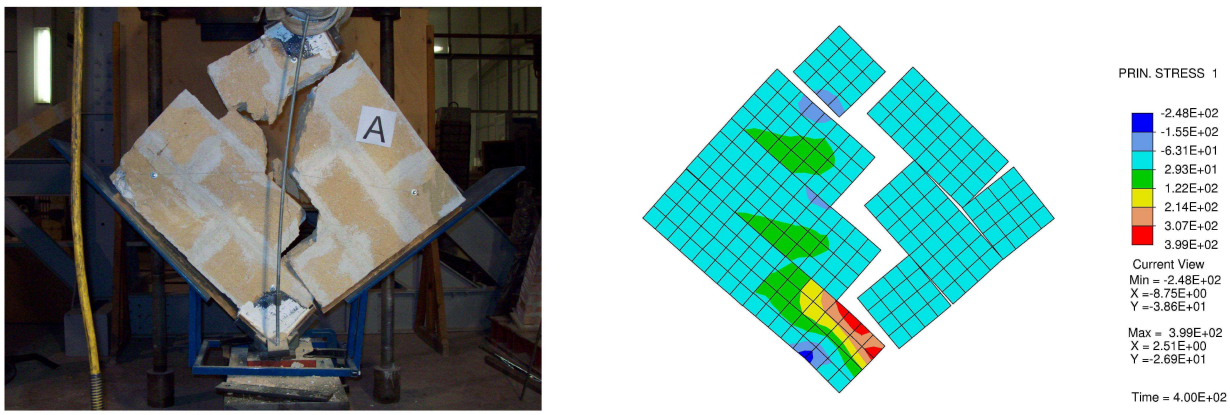

Figure 7. Comparison between numerical and experimental collapse configurations.

5. Conclusions.

The present paper deals with the mesomodelling of heterogeneous structures by means of interphase elements, that can be considered as an enhancement of the common interface elements. The possibility to distinguish internal and external contact stresses and strains permits to introduce separate failure conditions for the bulk material and for contact tractions. In particular an isotropic

damage model has been used to model the nonlinear response of the bulk material, while an elastoplastic bilinear domain governs the evolution of plasticity for contact tractions. The interphase model has been written in the framework of a thermodynamically consistent theory. State equations and flow rules have been derived and rewritten in a discrete form to be suitable to be used for finite element implementation. Two numerical applications on masonry structural elements have been conducted. In particular a compression test and a diagonal test have been carried out.
Ongoing and future efforts are devoted to the introduction of plastic activation functions on the physical interfaces between mortar and block, and to the possibility to introduce a new damage model to catch horizontal fractures also.

Acknowledgements

The authors acknowledge the financial support given by the Italian Ministry of Education, University and Research (MIUR) under the PRIN09 project 2009XWLFKW_005 , “A multiscale approach for the analysis of decohesion processes and fracture propagation”.

References

[1] G. Giambanco, S. Rizzo, R. Spallino, Numerical analysis of masonry structures via interface models. Comput. Methods Appl. Mech. Engrg., 190 (2001) 6493-6511.
[2] G. Alfano, E. Sacco, Combining interface damage and friction in a cohesive-zone model. Int. J. Numeric. Methods Engrg., 68 (2006) 542-582.
[3] I. Einav, G. T. Houlsby, G. D. Nguyen, Coupled damage and plasticity models derived from energy and dissipation potentials. Int. J. Solids Struct., 44 (2007) 2487-2508.
[4] M. R. Salari, S. Saeb, K. J. William, S. J. Patchet, R. C. Carrasco, A coupled elastoplastic damage model for geomaterials. Comput. Methods Appl. Mech. Engrg., 193 (2004) 2625-2643.
[5] P. B. Lourenco, J. Rots, Multisurface interface model for analysis of masonry structures. Journal Engrg. Mech., 123 (7) (1997) 660-668.
[6] A. Spada, G. Giambanco, P. Rizzo, Damage and plasticity at the interfaces in composite materials and structures. Comput. Methods Appl. Mech. Engrg., 198 (2009) 3884-3901.
[7] G. Alfano, M. A. Crisfield, Finite element interface models for the delamination analysis of laminated composite: mechanical and computational issues. Int. J. Numer. Meth. Engrg., 50 (2001) 1701-1736.
[8] K. William, I. Rhee, B. Shing, Interface damage model for thermomechanical degradation of heterogeneous materials. Comput. Methods Appl. Mech. Engrg., 193 (2004) 3327-3350.
[9] H. R. Lofti, P. B. Shing, Interface model applied to fracture of masonry structures. J. Struct. Eng. (ASCE), 120 (1) (1994) 63-80.
[10] F. Parrinello, B. Failla, G. Borino, Cohesive-frictional interface costitutive model. Int. J. Solids and Structures, 46 (2009) 2680-2692.
[11] G. Giambanco, Z. Mroz, The interphase model for the analysis of joints in rock masses and masonry structures. Mechanica, 36 (1) (2011) 111-130.
[12] G. Giambanco, G. Fileccia Scimemi, A. Spada, The interphase element. Comp. Mech., 50 (3) (2012) 353-366.
[13] E. Sacco, F. Lebon, A damage-friction interface model derived from micromechanical approach. Int. J. Solids and Structures, 49 (26) (2012) 3666-3680.